SOME ASPECTS OF DYNAMIC COMPUTATIONAL MODELLING OF DIRECT CURRENT PLASMA ARC PHENOMENA

QUINN G. REYNOLDS[*] AND B. DAYA REDDY[†]

[*] Pyrometallurgy Division
Mintek
Private Bag X3015, Ranburg 2125, South Africa
e-mail: quinnr@mintek.co.za, http://www.mintek.co.za/Pyromet

[†] Centre for Research in Computational and Applied Mechanics (CERECAM)
University of Cape Town
Private Bag X3, Rondebosch 7701, South Africa
email: daya.reddy@uct.ac.za, http://www.cerecam.uct.ac.za

Key words: Direct Current Furnace, Plasma Arcs, Dynamic Modelling

1 INTRODUCTION

Direct current arc furnaces see considerable use in modern industrial melting and smelting processes. Pyrometallurgical applications for this type of furnace are wide-ranging, and include commodities such as Ferrochrome, Ferronickel, Cobalt, Zinc, Magnesium, Titanium Dioxide, Platinum-group metals[1], and others.

Central to the operation of such furnaces is the direct current plasma arc, a sustained high temperature jet of ionised gas which is formed between the end of one or more graphite electrodes and the bath of molten process material below. Passage of electric current through the arc inputs energy and maintains the high temperatures necessary for ionisation via ohmic heating. This is balanced by various mechanisms of energy loss from the arc, including volumetric radiation and convection to the molten bath surface below. Much of this energy is delivered to a localised area directly beneath the arc, making it a very efficient means of heating the process material.

Flow of plasma in the arc column is driven strongly by electromagnetic Lorentz forces resulting from the constriction of the conduction channel in the vicinity of the electrode. This constriction causes the arc to draw in gas from the surroundings and accelerate it away from the electrode surface, toward the molten bath below (the Maecker effect[2]).

Much research has been conducted in the area of numerical modelling of arc phenomena, starting with Szekely and co-workers[3] and becoming increasingly more sophisticated with the advent of better software, property data, and increased computing capability. However, the majority of arc modelling efforts concentrate on steady-state, axisymmetric systems. While valuable from an engineering standpoint these models are not able to describe any transient behaviour exhibited by the arc, or any evolution of the shape and structure of the arc which breaks the symmetry imposed by the model. Both of these aspects are important for a deeper understanding of direct current plasma arc behaviour.

2 MATHEMATICAL MODEL

The direct current plasma arc is a coupled multiphysics system, requiring distributed parameter models of fluid flow, energy transfer, and electromagnetics. All these fields must be approximated by mathematical expressions and solved simultaneously in order to achieve an overall model of the arc.

As the arc is a high-velocity gas jet, it is fundamentally a fluid flow problem. For simplicity and in order to focus on the dynamic aspects of the arc behaviour, incompressible flow with constant physical properties is assumed. In this case the Navier-Stokes and continuity equations governing fluid flow reduce to:

$$\frac{\partial v}{\partial t} + (v \cdot \nabla)v + \nabla p = \nu \nabla^2 v + \frac{j \times B}{\rho} \tag{1}$$

$$\nabla \cdot v = 0 \tag{2}$$

In these equations, v is the fluid velocity vector, p is the reduced pressure (P/ρ), ν is the dynamic viscosity, ρ is the density, j is the current density vector, and B is the magnetic field vector. The momentum source term is the Lorenz force, which arises due to the interaction of magnetic and electric fields in the plasma. This provides strong coupling between the velocity and electromagnetic fields in the model.

In order to make (1) more amenable to numerical treatment, the gauge method formulation of E and Liu[4] is used. By defining auxiliary vector field a and gauge variable θ such that:

$$a = v + \nabla \theta \tag{3}$$

$$p = \frac{\partial \theta}{\partial t} - \nu \nabla^2 \theta \tag{4}$$

and substituting into (1) and (2) produces:

$$\frac{\partial a}{\partial t} + (v \cdot \nabla)v = \nu \nabla^2 a + \frac{j \times B}{\rho} \tag{5}$$

$$\nabla^2 \theta = \nabla \cdot a \tag{6}$$

v is recovered from the additional fields by a simple calculation using (3). A key strength of the gauge method over other primitive variable formulations is that boundary conditions for both a and θ may be unambiguously specified by using the gauge freedom. For example, a non-slip wall condition ($v = 0$ at boundary) may be written as:

$$\frac{\partial \theta}{\partial n} = 0, a \cdot n = 0, a \cdot \tau = \frac{\partial \theta}{\partial \tau} \tag{7}$$

Energy transfer in the direct current plasma arc model is treated using several simplifying assumptions. Firstly, the plasma fluid is considered to be in local thermodynamic equilibrium (LTE)[5], as a result of which a single temperature can be used to characterise the energy content of the material. LTE requires that the plasma be optically thin, dominated by reversible collision reaction processes, and exhibit small local gradients of plasma properties. The thermal plasmas found in direct current arc furnaces generally meet these conditions, although deviations can occur near to cold surfaces. In addition to LTE the physical properties of the plasma are assumed to be constant, as for the flow equations. With this, the energy conservation equation becomes:

$$\frac{\partial T}{\partial t} + \boldsymbol{v} \cdot \nabla T = \alpha \nabla^2 T + \frac{\boldsymbol{j} \cdot \boldsymbol{j}}{\sigma \rho C_P} - \frac{Q_R}{\rho C_P} \qquad (8)$$

Here, T is the plasma temperature, α is its thermal diffusivity, C_P is its heat capacity, σ is its electrical conductivity, and Q_R is the volumetric rate of radiative energy loss. Both σ and Q_R are strong functions of temperature and plasma composition, as shown for an air plasma[5,6] in Figures 1 and 2. Temperature is coupled to the velocity field via the convection term, and to the electromagnetic fields by the ohmic heating source term.
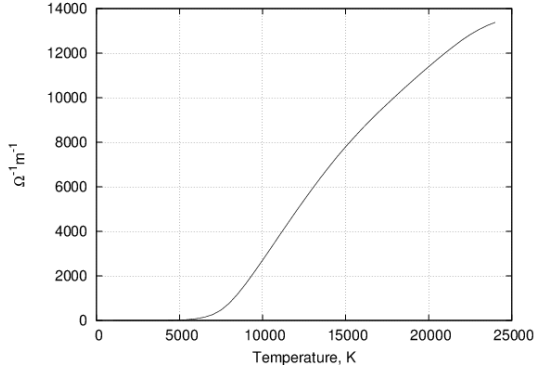

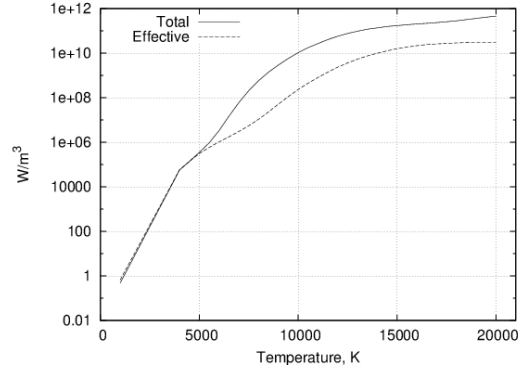**Figure 1**: σ of air as a function of temperature

Figure 2: Q_R of air as a function of temperature

The electromagnetic field components in the plasma arc model are modelled using Maxwell's equations, simplified for the case of a neutral medium. Since the time scales involved in plasma arc motion are much longer than those relevant to the transient terms in Maxwell's laws (in which field propagation occurs at the speed of light), the electrostatic and magnetostatic versions of the laws are used. The peak velocities in the arc jet are also assumed to be low enough to ignore the induced current due to fluid motion. With these approximations, we have from charge continuity:

$$\boldsymbol{j} = -\sigma \nabla \phi \qquad (9)$$

$$\nabla \cdot (\sigma \nabla \phi) = 0 \qquad (10)$$

In these relationships, ϕ is the electric potential field. Boundary conditions for the electric field are a combination of Dirichlet (specified potential, for eg. molten bath surface at ground = 0) and Neumann (specified current, for eg. electrically insulating surfaces, or fixed current densities at arc root) types.

The magnetic field is calculated from the current density distribution, once it is known. Ampere and Gauss's laws govern the magnetic field behaviour:

$$\nabla \times \boldsymbol{B} = \mu_0 \boldsymbol{j} \qquad (11)$$

$$\nabla \cdot \boldsymbol{B} = 0 \qquad (12)$$

These may then be reformulated using the magnetic vector potential, $\boldsymbol{A}$, such that:

$$\boldsymbol{B} = \nabla \times \boldsymbol{A} \qquad (13)$$

Substituting into (11) and applying the Coulomb gauge for $\boldsymbol{A}$ then gives:

$$\nabla^2 \boldsymbol{A} = -\mu_0 \boldsymbol{j} \qquad (14)$$

This expression is more amenable to numerical treatment, as it decouples the vector

1241

components of the magnetic field into three independent Poisson equations. Boundary conditions are imposed on (14) using the assumption that the boundary surfaces are magnetically insulating, only permitting lines of magnetic flux to pass into or out of the calculation region on parts of the boundary through which current is flowing:

$$A \cdot \tau = 0, \frac{\partial (A \cdot n)}{\partial n} = 0 \qquad (15)$$

It is interesting to note that as a result of the electromagnetic relationships, the Lorentz force term in (1) can be shown to be irrotational in two-dimensional cartesian coordinates. This can pose problems[7] for solutions of the plasma arc model in 2D. Fortunately these can be avoided by using a simple modification in the numerical treatment of (14), considering the calculation region for the magnetic field as though it has a small finite thickness in the third dimension. This results in the expression for (14) changing to the following, for 2D cartesian problems only:

$$\nabla^2 A - \frac{2A}{\delta L^2} = -\mu_0 j \qquad (16)$$

The size of the correction factor δL is specified in accordance with the dimensions of the arc column at its base, that is, where it attaches to the surface of the graphite electrode. This ensures that the magnitude and functional form of the magnetic field in the vicinity of the arc root, where the Lorentz force takes on its largest values, is accurate and physically realistic.

The calculation region and boundaries for the direct current plasma arc model are shown in Figures 3 and 4. A rectangular region immediately surrounding the arc in the central area of the furnace is modelled, consisting of the gas space between the tip of the graphite electrode and the top surface of the molten bath.
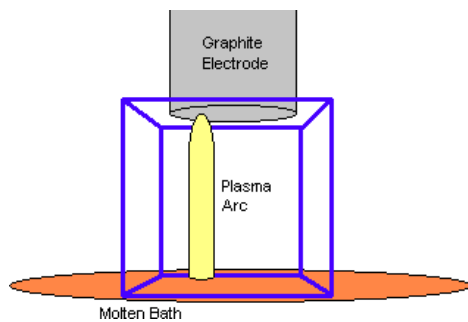
Figure 3: Solution region for arc models
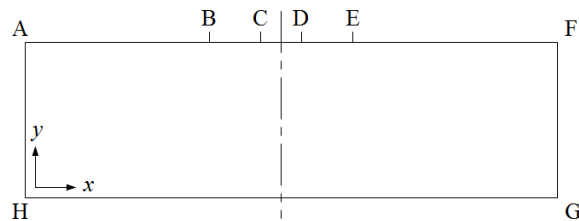
Figure 4: Region geometry (for 2D models)

In Figure 4, the origin of a cartesian coordinate system is located at H. The molten bath anode is located at surface GH, and the surface of the graphite electrode is section BE. The cathode spot, which forms the root of the arc column, is at CD. The remaining boundaries are treated as solid walls, forming a closed system.

The boundary conditions for the plasma arc model (in 2D) are shown in Table 1. The current density at the root of the arc on the surface of the graphite electrode, j_k, is governed by thermionic emission from the hot electrode, and has been determined experimentally[8] to be of the order of 3.5 x 10^7 A/m^2. Together with a specified total current, this determines the dimensions of the cathode spot at CD.

Table 1: Boundary conditions for plasma arc model

	CD	BC & CE	AH & FG	AB & EF	GH
$\boldsymbol{v}$	$v_x = v_y = 0$	$v_x = v_y = 0$	$v_x = v_y = 0$	$v_x = v_y = 0$	$v_x = v_y = 0$
θ	$\dfrac{\partial\theta}{\partial y} = 0$	$\dfrac{\partial\theta}{\partial y} = 0$	$\dfrac{\partial\theta}{\partial x} = 0$	$\dfrac{\partial\theta}{\partial y} = 0$	$\dfrac{\partial\theta}{\partial y} = 0$
$\boldsymbol{a}$	$a_y = 0, a_x = \dfrac{\partial\theta}{\partial x}$	$a_y = 0, a_x = \dfrac{\partial\theta}{\partial x}$	$a_x = 0, a_y = \dfrac{\partial\theta}{\partial y}$	$a_y = 0, a_x = \dfrac{\partial\theta}{\partial x}$	$a_y = 0, a_x = \dfrac{\partial\theta}{\partial x}$
T	$T = T_E$	$T = T_E$	$T = T_W$	$T = T_W$	$T = T_A$
ϕ	$\dfrac{\partial\phi}{\partial y} = -\dfrac{j_k}{\sigma}$	$\dfrac{\partial\phi}{\partial y} = 0$	$\dfrac{\partial\phi}{\partial x} = 0$	$\dfrac{\partial\phi}{\partial y} = 0$	$\phi = 0$
A	$A_x = \dfrac{\partial A_y}{\partial y} = 0$	$A_x = \dfrac{\partial A_y}{\partial y} = 0$	$A_y = \dfrac{\partial A_x}{\partial x} = 0$	$A_x = \dfrac{\partial A_y}{\partial y} = 0$	$A_x = \dfrac{\partial A_y}{\partial y} = 0$

The boundaries in the model are specified as having constant temperatures T_E, T_W, and T_A. These are the temperatures at the electrode, surrounding walls, and molten bath surface respectively. It is not physically unrealistic to have these surfaces at constant temperature, since in general the temperatures in the arc column are high enough to cause vapourisation of the materials they are made of; this process would be expected to hold the surfaces at the temperature of the phase change.

3 NUMERICAL METHOD

The numerical treatment of the direct current plasma arc model was approached with the aim of studying qualitative, time-dependent evolution of arc systems in mind. High spatial and temporal resolution as well as high performance were desirable, and led to the selection of finite difference methods together with explicit forward time-stepping techniques for the discretisation of the governing equations.

Structured cartesian grids with constant grid spacing were used in both 2D and 3D in an attempt to impose as little symmetry on the problem as possible, and to improve numerical performance. All spatial derivative terms are discretised using second-order centered differences, and a staggered grid is employed for certain fields such as $\boldsymbol{a}/\boldsymbol{v}$ and $\boldsymbol{j}$.

The time dependence of the governing equations is treated using a combination of methods. The flow equations are stepped forward in time using an explicit fourth order Runge-Kutta (RK4) algorithm. This imparts stability even at high Reynolds numbers[9], and results in relatively low computational cost per time step. Assuming ∇_h and Δ_h are the discrete equivalents of the Nabla and Laplace operators respectively, this may be written as:

$$\frac{\boldsymbol{a}_1 - \boldsymbol{a}_t}{\frac{1}{2}\delta t} + \left(\boldsymbol{v}_t \cdot \nabla_h\right)\boldsymbol{v}_t = \nu\Delta_h\boldsymbol{a}_t + \frac{\boldsymbol{j}_t \times \boldsymbol{B}_t}{\rho}, \quad \Delta_h\theta = \nabla_h \cdot \boldsymbol{a}_1, \quad \boldsymbol{v}_1 = \boldsymbol{a}_1 - \nabla_h\theta \qquad (17a)$$

$$\frac{\boldsymbol{a}_2 - \boldsymbol{a}_t}{\frac{1}{2}\delta t} + \left(\boldsymbol{v}_1 \cdot \nabla_h\right)\boldsymbol{v}_1 = \nu\Delta_h\boldsymbol{a}_1 + \frac{\boldsymbol{j}_1 \times \boldsymbol{B}_1}{\rho}, \quad \Delta_h\theta = \nabla_h \cdot \boldsymbol{a}_2, \quad \boldsymbol{v}_2 = \boldsymbol{a}_2 - \nabla_h\theta \qquad (17b)$$

$$\frac{a_3 - a_t}{\delta t} + (v_2 \cdot \nabla_h)v_2 = \nu\Delta_h a_2 + \frac{j_2 \times B_2}{\rho}, \quad \Delta_h\theta = \nabla_h \cdot a_3, \quad v_3 = a_3 - \nabla_h\theta \tag{17c}$$

$$\frac{a_4 - a_t}{\delta t} + (v_3 \cdot \nabla_h)v_3 = \nu\Delta_h a_3 + \frac{j_3 \times B_3}{\rho} \tag{17d}$$

$$a_{t+\delta t} = \tfrac{1}{3}a_1 + \tfrac{2}{3}a_2 + \tfrac{1}{3}a_3 + \tfrac{1}{6}a_4 - \tfrac{1}{2}a_t, \quad \Delta_h\theta = \nabla_h \cdot a_{t+\delta t}, \quad v_{t+\delta t} = a_{t+\delta t} - \nabla_h\theta \tag{17e}$$

The major computational cost of this algorithm is four solutions of the Poisson equation, one for the θ variable at each fractional time step. Due to the regular, structured nature of the discretisation grid and the homogeneous boundary conditions for θ, fast spectral transform methods can be applied to achieve rapid direct Poisson solves.

Adaptive time stepping is applied as the flow field evolves. Assuming the size of the grid spacing in the model to be δx, this is calculated according to the constraints[9]:

$$\delta t < \frac{\delta x^2}{4\nu}, \quad \delta t < \frac{\delta x}{|v|_{max}} \tag{18}$$

Due to the very strong self-coupling that occurs in the energy conservation equation (8), it requires additional numerical treatment in order to perform in a stable manner. The convection/diffusion terms are separated from the source terms using first-order operator splitting; since the source terms contain no spatial derivatives, they may then be calculated in a semi-implicit way without generating significant computational overhead. The remaining terms are then treated using RK4 explicit time stepping, as for the momentum equations. Using an intermediate variable T^*, the source term fractional time step becomes:

$$\frac{T^* - T_t}{\delta t} = \frac{j_t \cdot j_t}{\sigma(T^*)\rho C_P} - \frac{Q_R(T^*)}{\rho C_P} \tag{19}$$

(19) may then be solved for T^* using the known relationships between temperature and the plasma conductivity, and volumetric radiation loss. This expression is not fully implicit, as the temperature can additionally affect the current density j via the conductivity, but the computational cost of recalculating the electromagnetic fields iteratively does not justify the small additional stability gains to be had.

Once T^* is known, it is used as the starting point for the calculation of the convection/diffusion terms. This is illustrated in (20) using explicit forward-Euler time stepping, although in practice RK4 is used to retain the stability features described earlier:

$$\frac{T_{t+\delta t} - T^*}{\delta t} + v \cdot \nabla_h T^* = \alpha\Delta_h T^* \tag{20}$$

As a result of the use of RK4 for the convection/diffusion components of the energy balance equation, an additional time step size constraint is introduced:

$$\delta t < \frac{\delta x^2}{4\alpha} \tag{21}$$

This is used together with (18) to calculate the adaptive time step size during execution of the algorithm.

Solution of the pseudo-steady state electromagnetic field equations is required at each time step in the direct current plasma arc model. These equations have no time dependence, and must therefore be solved implicitly. The electric field equation (10) is discretised as:

$$\nabla_h \cdot (\sigma\nabla_h\phi) = 0 \tag{22}$$

The electrical conductivity is calculated from the most recent temperature field. The values of σ are required on the staggered grid, and so where interpolation between the grids is necessary, linear or bilinear methods are used. (22) is a non-constant coefficient problem and cannot be efficiently tackled with fast spectral methods; it is instead solved using a standard geometric multigrid algorithm. As the ϕ field is recalculated at least once every time step, and the time steps in the model are generally very small, a good initial estimate of the field is always available (the values from the previous step). Iterative multigrid with a preset number of cycles and relaxation steps was therefore chosen over the full multigrid algorithm.

Once the electric potential field is known, the current density field j may be calculated directly from it using the discrete version of (9).

The discretised versions of Poisson equations (14) and (16) governing the magnetic vector potential field A have constant coefficients and homogeneous boundary conditions, and are solved using rapid fast-spectral-method based solvers once the current density is known. The magnetic field is then calculated by taking the discrete curl of A.

The computational cost of the electromagnetic field calculation is high, comparable to the entire time step calculation for the remaining variables. They are therefore only recalculated once per time step (as opposed to once per RK4 stage). Together with the operator splitting of the energy equation this has the effect of reducing the temporal accuracy of the overall algorithm to first-order, although numerical testing suggests that the stability remains largely unaffected.

An overview of the algorithm used in the numerical solution of the direct current plasma arc model is shown in Figure 4.
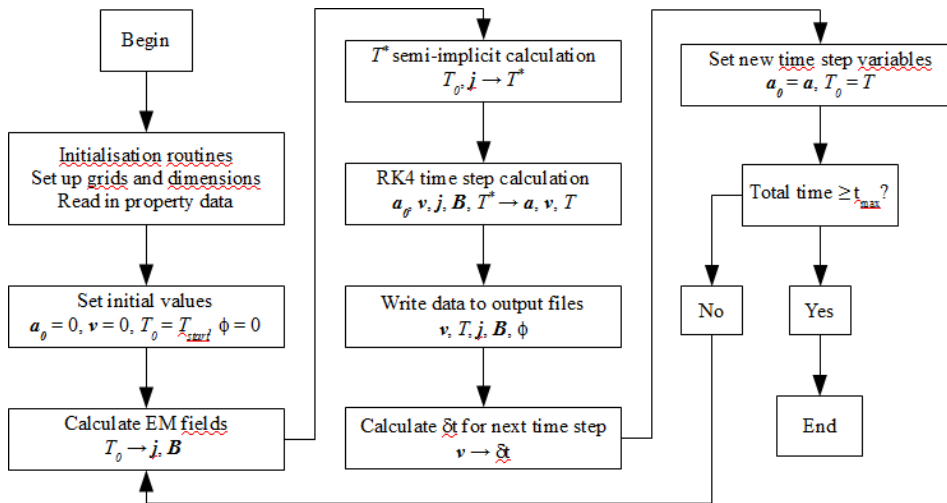

Figure 4: Direct current plasma arc model flowsheet

Implementation of the algorithm was performed using ANSI C. Outer loops of computationally intensive parts of the algorithm (particularly the fast spectral Poisson solvers and multigrid solver) were parallelised using OpenMP threading, providing increased performance on SMP machines. The Poisson solvers make extensive use of fast sine and cosine transforms provided by FFTW[10]. Extensive memory usage analysis and optimisation

was conducted to limit the memory footprint of the algorithm. Data sampling methods were implemented in order to reduce the quantity of file I/O during operation of the algorithm, which would otherwise be a rate-limiting step.

The implementation has been compiled and tested on a variety of computing platforms to date, including Intel (Pentium, Core2 and Xeon using gcc and icc compilers), IBM (P690 using xlc_r compilers), and Sun (SPARC M9000 using suncc compilers). Various flavours of Linux as well as Solaris have been successfully used as the host operating systems.

4 MODELLING RESULTS – 2D

Some results from an example case for the modelling of the direct current plasma arc system in two dimensions are presented below. The plasma gas used is air, for which phyiscal property information is readily available. The parameters used for the model are shown in Table 2.

Table 2: Parameters used for 2D arc model

Region dimensions	0.2 m x 0.05 m	Electrode width	0.05 m
ν	0.005040 m^2/s	Current	500 A
ρ	0.02593 kg/m^3	T_W, T_A, T_E	2000K, 3000K, 4100K
α	0.01256 m^2/s	Grid dimensions	1024 x 256
C_P	9420 J/kg.K	Model time	10 ms

Initial conditions of zero velocity and constant temperature of 10000K are applied throughout the calculation region.

At early stages of the simulation, the arc model forms a strong jet of plasma material directed away from the arc attachment spot on the electrode surface. The jet is initally stable and symmetric, however, this behaviour is not robust. Oscillations near to the arc root begin from approximately 0.6 ms resulting in the formation of strong vortices, which travel down the length of the arc column and break up the structure. The oscillating vortex production causes the arc to take on a somewhat sinusoidal shape.
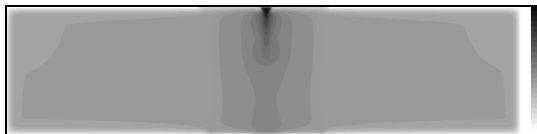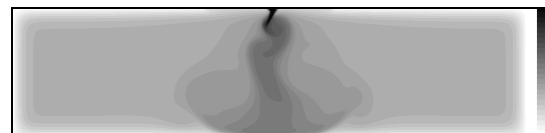

Figure 5: Temperature profile at 0.17 ms
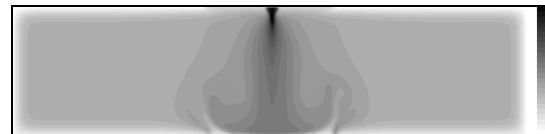
Figure 6: Temperature profile at 0.50 ms
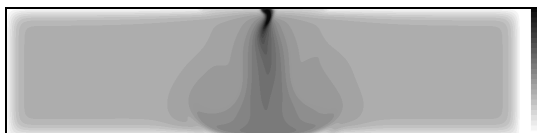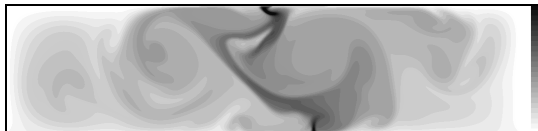

Figure 7: Temperature profile at 0.60 ms

Figure 8: Temperature profile at 0.70 ms

The process of arc jet formation and breakdown is shown in Figures 5 to 8. The

temperature profile is shown at various times, with the temperature scale ranging from 2000K (white) to 15000K (black).

Further into the simulation the arc jet becomes increasingly turbulent and chaotic in motion, forming a number of interesting structures as a result of the coupling between the flow field and the electromagnetic forces acting on it. One such phenomenon is the presence of persistent and highly-mobile arcs on the molten bath surface (which serves as anode in these models), shown in Figures 9 and 10. These are spontaneous emergent phenomena as the boundary conditions at this surface are entirely uniform, and have been confirmed experimentally using high speed photography[11].

Figure 9: Temperature profile at 7.80 ms, showing anode arcs and arc structure
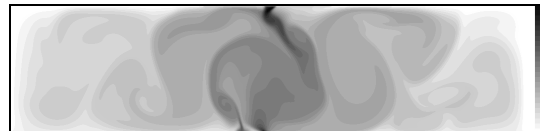
Figure 10: Temperature profile at 9.98 ms, showing anode arcs and arc structure

5 MODELLING RESULTS – 3D

The direct current plasma arc model is easily extended to three dimensions. This improves the spatial accuracy of the magnetic field and more accurately captures the qualitative geometry and behaviour of the arc, which is inherently a three-dimensional phenomenon. In the 3D models, the electrode surfaces and arc attachment spots are modelled as circular and may be located anywhere on the upper surface of the rectangular calculation region.

The 3D model is particularly well suited to the study of multiple arc systems. Some results from an example of this, a small twin-cathode furnace design with two electrodes and two arcs both carrying current in the same direction down to the molten bath anode, are shown below. Table 3 shows the parameters used for this model (where not given, parameters are identical to those given in Table 2).

**Table 3**: Parameters used for 3D arc model

Region dimensions	0.2m x 0.1m x 0.05m	Number of arcs	2
Grid dimensions	384 x 192 x 96	Current, arc 1	250 A
Arc separation	0.04 m	Current, arc 2	250 A

As in the 2D case, the twin-arc system initially forms stable arc jets directed away from the arc attachment spots. The onset of transient motion and decay of the pseudo-stable state occurs at approximately 1.5 ms. The nature of the subsequent motion is however considerably different, with the lower arc current causing the arc columns to settle into regular oscillations driven by precession of the arc jet around the attachment points on the electrode surfaces. This results in a dynamic helical structure forming within each arc column[11]. The macroscopic behaviour of the system is also interesting to observe, as the arcs attract each other by virtue of the current they carry. This attractive force draws the arc jets toward the centerline of the region, causing significant deflection of the arc columns in the process.

The three-dimensional temperature field is sampled by taking the maximum value along the y axis, producing a projected 2D temperature field in the x-z plane. These are shown for the early stages of the motion in Figures 11 to 14. The temperature scale runs between 2000K (white) and 15000K (black).
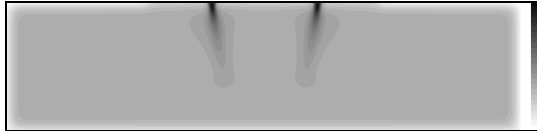
Figure 11: Projected temperature field at 0.5 ms
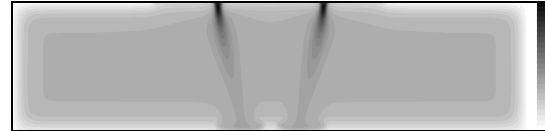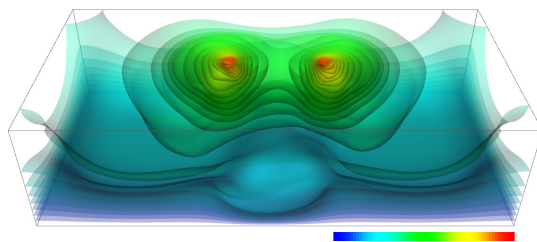

Figure 12: Projected temperature field at 1.0 ms
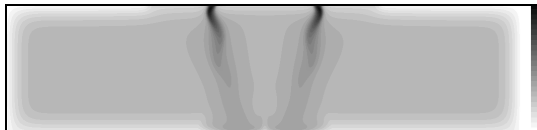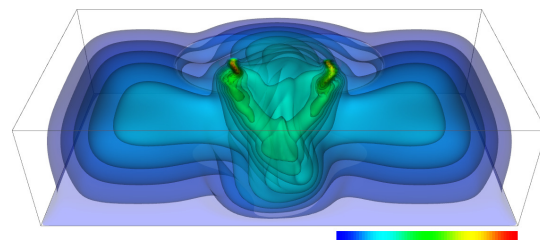

Figure 13: Projected temperature field at 1.5 ms

Figure 14: Projected temperature field at 2.0 ms

The full 3D fields for electric potential and temperature at the end of the simulation are shown in Figures 15 and 16. The scale ranges are 0 – 200 V and 2000 – 15000 K respectively.


Figure 15: Electric potential field at 10 ms

Figure 16: Temperature field at 10 ms

5.1 Transition effects with current

It is interesting to observe changes in the transient behaviour of the direct current plasma arc model as the various parameters are altered. One key parameter is the current carried by the arc(s), as this is an important operating variable for industrial direct-current arc furnaces.

The effect at low current was examined by changing the "Current, arc 1" variable in Table 3. Three different cases using values of 50 A, 100 A and 150 A were tested by completing simulation runs of the 3D model. The resulting projected temperature fields at the end of each simulation are shown in Figures 17 to 19, with scale range from 2000K (white) to 15000K (black). It can be seen that the low-current arcs, at left in each case, exhibit very different structure depending on the current. This is borne out in the temporal behaviour – Figure 20 shows the evolution of the arc voltage, which is defined as the local maximum value of the electric potential field in the vicinity of the arc attachment spot on the electrode surface, for the left-hand arc in each of the low current cases. There is a marked change in the transient arc behaviour between 100 and 150 A; at lower values, the arc voltage appears to remain approximately at steady state with only slow variations in time, while at higher currents, the

voltage begins to oscillate at a constant frequency. This reflects a change in the transient structure of the arc column, from a steady jet to a helical structure formed by precession of the jet around the arc attachment spot.
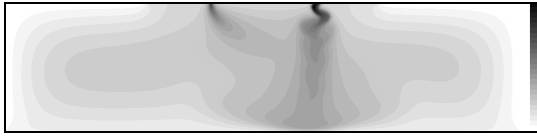
Figure 17: Projected temperature field,
left arc at 50 A, right arc at 250 A
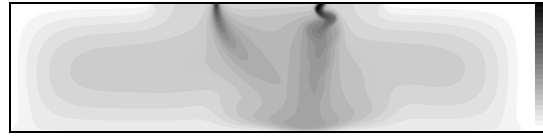
Figure 18: Projected temperature field,
left arc at 100 A, right arc at 250 A
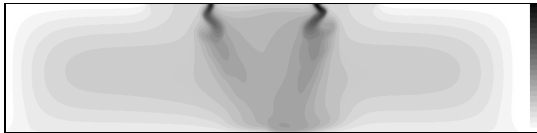
Figure 19: Projected temperature field,
left arc at 150 A, right arc at 250 A

In order to compare the nature of the transient behaviour of arcs in the model at higher currents, two additional cases of the twin-arc 3D model were tested. In both cases the "Arc separation" variable in Table 3 was set at 0.1 m, placing the arcs well apart to reduce their interaction. The first case was run with the arc currents at 250 A each, and the second was run with the currents at 500 A each. The second case also used a higher-resolution numerical grid, at 768 x 384 x 192 in size. A sample of the temporal behaviour of the arc voltage for the left-hand arc in each case is shown in Figure 21. The increased current is seen to produce considerably more more irregular and chaotic behaviour.
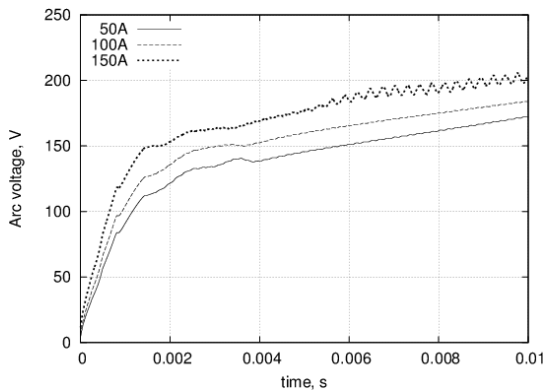
Figure 20: Evolution of arc voltage at low currents
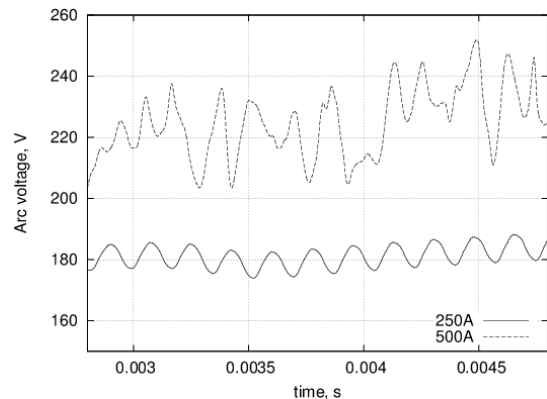
Figure 21: Evolution of arc voltage at higher currents

Multiple transition effects are therefore possible with variation of the current parameter in the direct current plasma arc model. Low currents produce steady arc jets, moderate currents produce regular oscillations in the system, and finally higher currents can produce erratic, complex motion. Similar transition effects have been observed experimentally using high speed photography[11], however much work remains to be done in this area.

6 CONCLUSIONS

The development of a dynamic model of direct current plasma arc systems of relevance to metallurgical furnace design has been largely successful. A novel solver algorithm using finite difference methods, explicit time-stepping, and rapid solver techniques has been produced, and is capable of scaling to large problem sizes on modest computing resources. The solver retains reasonable spatial and temporal accuracy while also possessing good stability properties.

Selected results from the model in both 2D and 3D show a variety of transient phenomena, including symmetry breaking in the early stages of arc formation, emergent behaviour such as spontaneous anode arc formation, and distinct transition effects with system parameters such as arc current.

Further avenues of research should include extension of the model to variable physical properties, induced current terms in the electromagnetic field equations, and compressible flow. Investigation of two-temperature plasma fluid models is also advised.

7 ACKNOWLEDGEMENTS

REFERENCES

[1] Jones, R.T. Towards commercialisation of Mintek's ConRoast process for platinum smelting, *Proceedings of the 48th Annual Conference of Metallurgists of CIM* (2009) 159-168

[2] Maecker, H. Plasmastromungen in Lichtbogen infolge Eigenmagnetische Kompression, *Zeitschrift fur Physik* (1955) **141**:198-216

[3] Ushio, M., Szekely J. and Chang C.W. Mathematical modelling of flow field and heat transfer in high-current arc discharge, *Ironmaking and Steelmaking* (1981) **6**:279-286

[4] E, W. and Liu, J.G. Gauge method for incompressible flows, *Communications in Mathematical Sciences* (2003) Vol. 1 **2**:317-332

[5] Boulos, M.I., Fauchais, P. and Pfender, E. *Thermal plasmas: fundamentals and applications*. Plenum Press, Vol. 1 (1994)

[6] Naghizadeh-Kashani, Y., Cressault, Y. and Gleizes, A. Net emission coefficient of air thermal plasmas, *Journal of Physics D: Applied Physics* (2002) **35**:2925-2934

[7] Mutschke, G. and Bund, A. On the 3D character of the magnetohydrodynamic effect during metal electrodeposition in cuboid cells, *Electrochemistry Communications* (2008) **10**:597-601

[8] Bowman, B. Properties of arcs in DC furnaces, *Proceedings of the 52nd Electric Furnace Conference* (1995) 111-120

[9] E, W. and Liu, J.G. Vorticity boundary condition and related issues for finite difference schemes, *Journal of Computational Physics* (1996) **124**:368-382

[10] http://www.fftw.org

[11] Reynolds, Q.G, Jones, R.T. and Reddy, B.D. Mathematical and computational modelling of the dynamic behaviour of direct current plasma arcs, *Proceedings of the 12th International Ferroalloys Congress* (2010) 803-814